Surface modification of carbon dots with tetraalkylammonium moieties for fine tuning their antibacterial activity

Elizaveta Sviridova, Alexandre Barras, Ahmed Addad, Evgenii Plotnikov, Antonio Di Martino, D. Deresmes, Ksenia Nikiforova, Marina Trusova, Sabine Szunerits, Olga Guselnikova, et al.

HAL Id: hal-03687095
https://hal.science/hal-03687095

Submitted on 7 Nov 2022

Journal Pre-proof

Surface modification of carbon dots with tetraalkylammonium moieties for fine tuning their antibacterial activity

Elizaveta Sviridova, Alexandre Barras, Ahmed Addad, Evgenii Plotnikov, Antonio Di Martino, Dominique Deresmes, Ksenia Nikiforova, Marina Trusova, Sabine Szunerits, Olga Guselnikova, Pavel Postnikov, Rabah Boukherroub
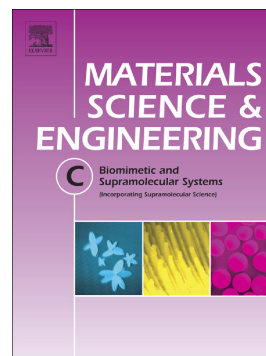
This is a PDF file of an article that has undergone enhancements after acceptance, such as the addition of a cover page and metadata, and formatting for readability, but it is not yet the definitive version of record. This version will undergo additional copyediting, typesetting and review before it is published in its final form, but we are providing this version to give early visibility of the article. Please note that, during the production process, errors may be discovered which could affect the content, and all legal disclaimers that apply to the journal pertain.

Surface modification of carbon dots with tetraalkylammonium moieties for fine tuning their antibacterial activity

Elizaveta Sviridova[1], Alexandre Barras[2], Ahmed Addad[3], Evgenii Plotnikov[1], Antonio Di Martino[1], Dominique Deresmes[2], Ksenia Nikiforova[1], Marina Trusova[1], Sabine Szunerits[2], Olga Guselnikova[1], Pavel Postnikov[1, 4*], Rabah Boukherroub[2*]

[1] Research School of Chemistry and Applied Biomedical Sciences, Tomsk Polytechnic University, 634050 Tomsk, Russian Federation

[2] Univ. Lille, CNRS, Centrale Lille, Univ. Polytechnique Hauts-de-France, IEMN, UMR CNRS 8520, F-59000 Lille, France

[3] Univ. Lille, CNRS, UMR 8207 – UMET, F-59000 Lille, France

[4] Department of Solid-State Engineering, University of Chemistry and Technology, 16628 Prague, Czech Republic

Corresponding authors:

Pavel Postnikov, Tel. +79039136029 (postnikov@tpu.ru);

Rabah Boukherroub, Tel. +330362531724 (rabah.boukherroub@univ-lille.fr)

1

Abstract

The widespread of bacterial infections including biofilms drives the never-ending quest for new antimicrobial agents. Among the great variety of nanomaterials, carbon dots (CDs) are the most promising antibacterial material, but still require the adjustment of surface properties for enhanced activity. In this contribution, we report a facile functionalization method of carbon dots (CDs) by tetraalkylammonium moieties using diazonium chemistry to improve their antibacterial activity against Gram-positive and Gram-negative bacteria. CDs were modified by novel diazonium salts bearing tetraalkylammonium moieties (TAA) with different alkyl chains (C2, C4, C9, C12) for the optimization of antibacterial activity. Variation of the alkyl chain allows to reach the significant antibacterial effect for CDs-C9 towards Gram-positive *Staphylococcus aureus (S. aureus)* (MIC=3.09 ± 1.10 µg mL^{-1}) and Gram-negative *Escherichia coli (E. coli)* (MIC=7.93 ± 0.17 µg mL^{-1}) bacteria. The antibacterial mechanism of CDs-C9 is ascribed to the balance between the positive charge and hydrophobicity of the alkyl chains. TAA moieties are responsible for enhanced adherence on the bacterial cell membrane, its penetration and disturbance of physiological metabolism. CDs-C9 were not effective in the generation of reactive oxygen species excluding the oxidative damage mechanism. In addition, CDs-C9 effectively promoted the antibiofilm treatment of *S. aureus* and *E. coli* biofilms ou performing previously-reported CDs in terms of treatment duration and minimal inhibitory concentration. The good biocompatibility of CDs-C9 was demonstrated on mouse fibroblast (NIH/3T3), HeLa and U-87 MG cell lines for concentrations up to 256 µg mL^{-1}. Collectively, our work highlights the correlation between the surface chemistry of CDs and their antimicrobial performance.

Keywords: Carbon dots; diazonium chemistry; tetraalkylammonium salts; antibacterial activity; biofilms

1. Introduction

There is a global challenge in the overcoming of bacterial resistance caused by increasingly ineffectiveness of common antibiotic molecules - in 2019, only 6 of 32 clinical developed antibiotics were classified as innovative [1]. In most cases, all the current antibiotics are not able to treat bacteria biofilms that are responsible for causing a broad range of chronic diseases [2]. Therefore, there is an urgent need to develop new alternative antimicrobial agents to prevent extending drug-resistance and biofilm-related infections.

In the last decade, great attention has been focused on the development of nanomaterials with antimicrobial properties including antibiofilm characteristics [3,4]. Recent investigations on efficiency of noble metal nanoparticles [5,6], semiconductor nanoparticles [7–9], 2D materials [10,11], metal-organic frameworks [12,13] and carbon-based nanomaterials [14,15] as antibacterial agents have represented a worth potential for the treatment of bacterial infection. However, the application of metal-based nanomaterials is hindered by bio-toxicity, high cost and even emergence of bacterial drug resistance [16]. The application of semiconductor nanomaterial, 2D and 3D materials is limited by potential health risks related to the antibacterial effect: finite lifespan, action radius of ROS, and risk of normal tissues damage in the case of higher ROS production and hyperthermia. That has opened the door for wide practical application of carbon-based antibacterial agents, particularly, carbon dots (CDs). CDs are highly attractive due to their structural features associated with "zero-dimensional" size. CDs can be readily prepared by environmentally-friendly and low-cost methods. Particularly important is that CDs form stable aqueous suspensions and are non-toxic nanomaterials, especially in comparison with metal nanoparticles [5,6]. These features make CDs one of the close-to-perfect platforms for wide applications in the healthcare field.

The application of CDs as antibacterial agents is often limited by their low activity in pristine form. In order to enhance the efficacy of antibacterial treatment, the implementation of special synthetic or post-synthetic modification procedures is required [17,18]. A widespread method for the synthesis of antibacterial active CDs is based on the solvothermal treatment of nitrogen-rich feedstock [19–24]. All these N-containing precursors enhance the affinity to the bacteria membrane and further killing *via* electrostatic/hydrophobic interactions, generation of reactive oxygen species (ROS) or DNA/RNA damage [22,25]. Nevertheless, the solvothermal approaches do not allow to fine tune the surface properties and predict the properties of the produced CDs.

A more careful control of the surface properties and functionality can be achieved using surface modification methods [19]. Among the different functionalization schemes [26–28], diazonium

3

chemistry is highly appealing owing to the high reactivity of diazonium salts, versality of chemical structure and formation of strong covalent bonds with the surface [29–32]. CDs can be readily functionalized by aryl radicals, generated from appropriate diazonium salts, which allow to introduce specific surface properties [33,34]. Unfortunately, the diazonium surface chemistry has been widely applied for the modification of surfaces for sensing related aspects [35,36] as well for stabilization of graphene suspensions [37,38], but not for endowing nanomaterials with antibacterial properties [35,36,39].

In this contribution, we propose a versatile approach for the surface modification of CDs by novel diazonium salts bearing tetraalkylammonium moieties (**TAA**) of different alkyl chain lengths. Variation of the alkyl chain length allows to establish a relationship between the structure of surface functional groups and antibacterial performance for the preparation of effective antibacterial agents for both Gram-positive (*Staphylococcus aureus*) and Gram-negative (*Escherichia coli)* bacteria and their biofilms. To the best of our knowledge, this study represents the first report on CDs functionalization with diazonium salts bearing quaternary ammonium moieties with varying alkyl chain lengths for antibacterial and antibiofilm applications, opening more opportunities for the application of CDs in the field of biomedicine.

2.   Experimental part

2.1 Synthesis of amine-functionalized carbon dots (CDs)

CDs were synthesized following a slightly modified method reported in [26]. In brief, citric acid (2.1 g) and ethylenediamine (670 μL) were dissolved in Milli-Q water (20 mL). Then, the solution was transferred in a 30 mL reaction vessel of a microwave reactor (Monowave 450, Anton-Paar). A total of 2 min was required to elevate the temperature of the reaction vessel up to 200°C and maintained at this temperature for 5 min and then cooled to room temperature (20-22°C). The resulting solution was dialyzed in DI water through a dialysis membrane (Biotech CE N°131093, MWCO = 500–1000 Da) for 24 h with changing MQ water every 3 h in order to remove unreacted small molecules. Then, a dry mass of 200 μL solution was weighted by microbalance (XPR6UD5, Mettler Toledo) for the estimation of the concentration.

2.2 Modification of carbon dots with diazonium salts (CDs-C2, CDs-C4, CDs-C9 and CDs-C12)

A solution of freshly synthesized CDs (1 mL, 2 mg mL^{-1}) in water was mixed with methanol (water for CDs-C2) solution of ADT-N$^+$(Alk)$_3$ (1 mL, 12 mg mL^{-1}), ultrasonicated for 1 h and stirred for 3

h at room temperature (20-22°C). Then, the desired product (CDs-C2, CDs-C4, CDs-C9 and CDs-C12) was purified by dialysis against MQ water during 24 h using 3.5 kDa regenerated cellulose membrane [30].

CDs-C4, CDs-C9 and CDs-C12 were additionally purified twice for removing unreacted diazonium salts by centrifugation (8000 rpm, 20 min) after dialysis and dissolution in water prior to lyophilization.

2.3 Characterization of CDs and modified CDs (Mod-CDs)

Size and zeta-potential measurements were performed using a Zetasizer Nano-ZS (Malvern Instruments Inc. Worcestershire, UK). CDs and Mod-CDs (10 µg mL^{-1}) were diluted in type 1 ultrapure water at pH 7.0.

Atomic force microscopy (AFM) measurements (Bruker Dimension 3100) were carried out in ambient air, in the tapping (Intermittent contact) mode, using commercial standard silicon tip with a radius of approximately 10 nm (Bruker NCHV-A). The sample was prepared by dropping an aqueous CDs or Mod-CDs suspension onto a freshly cleaved mica surface and dried at ambient temperature.

UV-vis spectroscopic measurements were carried out using a SAFAS UVmc2 spectrophotometer (Safas S.A., Monaco) operating at a resolution of 1 nm. The UV−vis spectra were recorded in quartz cuvettes of 1 cm path length between 200 and 600 nm.

Emission and excitation fluorescence spectra were recorded between 250 and 650 nm using a Xenius XC spectrofluorometer (Safas S.A., Monaco). Fluorescence measurements of CDs (30 µg mL^{-1}) were performed in water (excitation and emission bandwidth=10 nm, step=1 nm, PMT voltage=270 V, scan).

Fourier-transform infrared (FTIR) spectra were recorded using a ThermoScientific FTIR instrument (Nicolet 8700) in the range between 650 and 4000 cm^{-1} at a spectral resolution of 4 cm^{-1}. 1 mg of dried CDs or Mod-CDs was mixed with 200 mg of KBr powder in an agar mortar. The mixture was pressed into a pellet under 7 tons of load for 2–4 min, and the spectrum was recorded immediately. A total of 64 accumulative scans were collected. The signal from a pure KBr pellet was subtracted as a background.

X-ray photoelectron spectroscopy (XPS) measurements were performed with a Theta Probe spectrometer (Thermo Fisher Scientific) using a monochromatic Al Kα X-ray source (1486.6 eV) under a vacuum of about 2×10^{-6} Pa at a photoelectron take-off angle of 45°.

Transmission electron microscopy (TEM) and high resolution TEM (HRTEM) were investigated by using a FEI TECNAI G2-20 operated at an accelerating voltage of 200 kV with a resolution of 1.9 Å.

2.4 Quantum yield measurements

The fluorescence quantum yields of pristine and Mod-CDs were determined by the slope method [40], by comparing the integrated photoluminescence intensity and absorbance of each sample with that of a reference. Quinine sulfate (in 0.1 M H_2SO_4 as a solvent; QY = 0.54) was chosen as the reference. The quantum yield was calculated using the following equation:

$$\phi_x = \phi_{st} (K_x/K_{st}) (\eta_x/\eta_{st})^2$$

where ϕ is the quantum yield, K is the slope determined by the curves and η is the refractive index of the solvent. The subscript "st" refers to the standard with the known quantum yield and "x" for the sample. In order to minimize re-absorption effects, absorption in the 10-mm fluorescence cuvette was kept below 0.10 at the excitation wavelength (350 nm). For these aqueous solutions, $\eta_x/\eta_{st} = 1$. A series of concentrations of the reference and sample were measured to obtain the slopes of the curves.

2.5 Cell culture, cytotoxicity assay and cellular uptake

2.5.1 Cytotoxicity assay

In vitro cytocompatibility of pristine and modified CDs was assessed on mouse embryonic fibroblast 3T3-L1 (ATCC CL-173™ NIH/3T3), following a standard protocol already reported in a previous work [41]. Cytotoxicity test was conducted according to the EN ISO 10993-5 standard with modification. Dulbecco's Modified Eagle's Medium (Gibco, USA) containing 10% calf serum (One Shot ™, Thermo Fisher Scientific, Brazil), supplemented with glutamine supplement (GlutaMAX, Gibco, USA), and penicillin/streptomycin at 100 U/mL (Paneko, Russia) was used as culture medium. The CDs were diluted to concentrations from 0 to 64 μg mL^{-1} (for 24 h) and to 512 μg mL^{-1} (for 2 and 6 h) in the culture medium. The cells were pre-cultivated for 24 h, and the culture medium was subsequently replaced with dilutions of the samples. As a reference, cultivation in pure medium without CD samples was carried out.

To assess the cytotoxic effect, MTT assay (Invitrogen Corporation) was performed after 2, 6 and 24 h of cell cultivation in the presence of the samples. All tests were conducted in quadruplicates. The absorbance was measured at 570 nm on an Multiskan™ FC Microplate Photometer – (Thermo Fisher Scientific). Dixon's Q test was applied to remove outlying values. Cell viability is displayed as the percentage of cells present in respective sample with CDs relative to cells cultivated in pure medium in absence of CDs (100% viability)

The HeLa [ATCC® CCL-2™, ECACC, Sigma Aldrich, Saint-Quentin Fallavier, France] and U-87 MG [ATCC® HTB-14™, ECACC, Sigma Aldrich, Saint-Quentin Fallavier, France] cell lines were cultured and maintained in Dulbecco's Modified Eagle's medium (DMEM, Gibco®) supplemented with 10% fetal bovine serum (FBS, Gibco®) and 1% penicillin-streptomycin (Gibco®) in a humidified incubator at 37°C and 5% CO_2. Cells were seeded at a density of 10^4 cells/well in a 96-well plate and grown for 24 h before assay. The culture medium was replaced with a fresh medium that contains the CDs. The final concentration of CDs, CDs-C2, CDs-C4, CDs-C9 and CDs-C12 in the well was 12.5, 25, 50 µg mL^{-1}. After 24 h, the old medium was aspirated and cells were washed three times with PBS. The cell viability was evaluated using Uptiblue (Interchim) method. Briefly, 100 µL of the resazurin solution (11 µg mL^{-1}) in DMEM with 10% FBS were added to each well and the plate was incubated for 4 h in the humidified incubator. The fluorescence emission of each well at 590 nm was measured using a microplate reader (PHERAstar FS, BMG LABTECH GmbH, Germany). Each condition was replicated five times and the mean absorbance value of non-exposed cells was taken as 100% cellular viability.

2.6 The antibacterial activity of pristine and modified CDs
2.6.1 Bacterial culture and preparation

The bacteria used in this study were *S. aureus* ATCC® 43300™ (Gram positive) and *E. coli* K12 MG1655 (Gram negative) strains. A single *E. coli* or *S. aureus* colony from LB/BHI agar plate was inoculated overnight in MHB medium at 37°C with moderate shaking. The pre-culture was diluted 50-fold and allowed to continue for another 3–4 h, until the optical density at 600 nm (OD$_{600}$) had reached 0.6–1.

2.6.2 Determination of minimum inhibition concentration

7

The pre-culture of *S. aureus* ATCC® 43300™ and *E. coli* K12 MG1655 (10^8 CFU mL^{-1}) was then diluted by 1:100 in MHB broth (10^6 CFU mL^{-1}). 50 µL of the bacterial suspension was then added to all wells containing CDs and to the control wells, resulting in 5×10^5 CFU mL^{-1}. To perform the minimum inhibition concentration (MIC) test, different concentrations (0.25, 0.5, 1, 2, 4, 8, 16, 32, 64, 128 µg mL^{-1}) of pristine and modified CDs were prepared by serial dilution into 96-well microplates containing 50 µL of the inoculum. The as-prepared bacterial suspensions were incubated at 37°C without shaking for 18-24 h. The MIC was determined by reading the OD$_{600}$ with the multiplate reader.

The lowest concentration (highest dilution) required to arrest the bacterial growth was regarded as the MIC value. All the concentration values were analyzed three times and the relative standard deviation was less than 1% [42].

The determination of MIC under light irradiation was investigated by irradiating a suspension of bacteria (10^6 CFU mL^{-1}) in the presence of CDs at different concentrations for 20 min at 0.41 W cm^{-2}.

2.7 Biofilm assay

2.7.1 Biofilm formation and quantification

S. aureus and *E. coli* bacteria strains were cultured in TSB at 37°C for approximately 3-4 h in order to reach mid-log phase (OD 0.5-0.6). Cells were pelleted by centrifugation (5000 g, 5 min, 20°C) then washed twice with Potassium Phosphate Buffer (PPB; 100 mM, pH 7). Bacterial suspensions were adjusted to 10^8 CFU mL^{-1} in PPB (OD 600 nm = 0.1) or to 10^9 CFU mL^{-1} in PPB (OD 600 nm = 1). Biofilm formation was initiated in 24-well plate (Nunclon™) by covering polystyrene (PS) surface with 1 mL of the cell suspension adjusted to 10^7 CFU mL^{-1} and incubated at 20°C for 2 h (*S. aureus)* and 3 h *(E. coli)* to allow the bacterial adhesion. Afterwards, the wells were rinsed with PPB, to remove loosely attached cells. Each well was covered with 2 mL of TSB and incubated statically at 37°C for 72 h (*S. aureus)* and 120 h *(E. coli)* (change medium every 24 h). After the biofilm matured, the grown biofilms were gently washed (3-4×) with PPB solution to remove any non-adherent bacteria for subsequent experiments [43,44].

Evaluation of biofilm formation was investigated by several methods: (1) crystal violet staining experiments; (2) direct brightfield microscopy; (3) live/dead staining assay.

(1) Crystal violet (CV) staining experiments: Briefly, the biofilms were fixed by 200 µL of methanol for 15 min, stained with 200 µL of CV solution (0.1 wt%) for 10 min, and washed with

8

PBS (3×) to remove the unbound dyes and dried for 15 min. Next, the biofilms were treated with 200 μL of ethanol for 15 min, and the biofilm biomass of each sample was quantified by measuring the absorbance at 570 nm using the microplate reader (Multi-mode reader, CYT5MV, Biotek). Each sample was tested in triplicate, and three independent experiments were performed. The same procedure for 3 control wells without any bacteria was carried out.

$$Biomass\ of\ biofilm = \frac{OD_{570nm}\ (sample)}{OD_{570nm}\ (control)} \times 100\ \%$$

(2) direct brightfield microscopy;

(3) Live/dead staining assay: Briefly, to investigate the states of bacteria in biofilms, live/dead staining assay was conducted using the LIVE/DEAD BacLight bacterial viability kit containing green-fluorescent SYTO 9 (Ex = 488 nm) and red-fluorescent nucleic acid dye (propidium iodide, PI, Ex = 552 nm). The culture media were replaced with PBS solutions containing SYTO 9 and PI dyes (1 μL+ 1 μL per 1 mL), which stained live bacteria in green and dead bacteria in red, respectively. The live/dead staining experiments were carried out according to the manufacturer's instructions. After that, the samples were imaged using a microscope (Multi-mode reader, CYT5MV, Biotek) with 20× objective magnification and with the corresponding excitation and emission filters (469-35/525-39 nm for SYTO^{TM} 9 and 586-15/647-57 nm for propidium iodide).

2.7.2 Biofilm destruction assay and quantification

The obtained biofilms of *S. aureus* and *E. coli* were incubated with 1 mL of different concentrations of CDs-C9 (0, 16, 32, 48, 64, 128, 256 μg mL^{-1}) for different times (2, 6 h) in PBS medium at 30°C, followed by washing (3-4×) the remaining biofilms with PPB.

Quantification:

(1) To intuitively observe the biofilm destruction performance, the treated and non-treated biofilms were covered by a solution of TSB approximately for 6-8 h for bacteria growth at 37°C (control OD$_{600}$ ~0.3-0.4). The bacteria growth of each biofilm was measured using the microplate reader at the absorbance of 600 nm [45].

(2) To investigate the states of bacteria in treated/non-treated biofilms, live/dead staining assay was conducted (described above).

(3) To evaluate the biomass of treated/non-treated biofilms, CV staining assay was performed (described above).

9

(4) Colony forming assay: Following the removal of the planktonic cells by washing with PPB, the wells were vigorously scratched from the surface with sticks, pipetted and carefully vortexed to disperse the biofilms. After being diluted with PPB, the samples (200 μL) were separately spread on agar plates (BHI agar for *S. aureus* and LB agar for *E. coli*). After incubation at 37°C for 18 h, the colony-forming units (CFU) formed on the plates were counted and photographed.

2.8 Mechanism investigation

2.8.1 Determination of reactive oxygen species (ROS) of CDs

In order to examine the production of intracellular ROS, 2′,7′-dichlorodihydrofluorescein diacetate (DCFH-DA) was used [23]. One colony from the plates was transferred into 3 mL TSB and incubated at 35 °C, 200 rpm in an orbital shaker incubator (Labnet 211DS) until it reached the exponential growth phase (OD600=0.5-1.0; GeneQuant pro, Amersham Biosciences). The cell suspensions were stained with 10 μM DCFH-DA (from DMSO solution) for 30 min and then washed once by centrifugation (3500 g for 5 min; Eppendorf 5804) with PBS (pH 7.4; Gibco®). The pellets were resuspended in PBS and the final bacterial concentration was adjusted to 10^7 CFU mL^{-1}. After that, the bacteria samples were treated with CDs (64 μg mL^{-1}) in PBS for 30 min. Treated cells, cells alone stained with DCFH-DA served as the negative controls and 1% H_2O_2 as the positive control. Relative fluorescence intensities were recorded in a 96-well cell culture plate from the bottom using a Cytation™ 5 Cell Imaging Multi-Mode Reader (BioTek Instruments SAS, France) at an excitation/emission wavelength of 485-20/528-57 nm.

2.8.2 Bacteria interaction study

The bacterial suspensions of *E. coli* or *S. aureus* (≈10^9 CFU mL^{-1}, 1.0 mL) were centrifuged (RCF 3000 g, 10 min, 25 °C) and washed twice with sodium phosphate buffer solution (PBS, pH 7.4). Aliquots of *S. aureus* and *E. coli* (10^7 CFU mL^{-1}) were cultured with CDs (128 μg mL^{-1}) for 15 min and washed with phosphate buffered solution (PBS, pH = 7.4). The samples were imaged using a microscope (Multi-mode reader, CYT5MV, Biotek) with 20× objective magnification and with the corresponding excitation and emission filters (469-35/525-39 nm).

2.8.3 The staining assay of live/dead bacteria

The bacterial suspensions of *E. coli* or *S. aureus* (≈10^9 CFU mL^{-1}, 1.0 mL) were centrifuged (RCF 3000 g, 10 min, 25 °C) and washed twice with sodium phosphate buffer solution (PBS, pH 7.4). Aliquots of *S. aureus* and *E. coli* (10^7 CFU mL^{-1}) were treated with CDs (CDs, CDs-C2 and CDs-

C4 at 256 μg mL^{-1} for both strains; CDs-C9 at 16 μg mL^{-1} for *S. aureus* and 32 μg mL^{-1} for *E. coli*; CDs-C12 at 128 μg mL^{-1} for *S. aureus* and 256 μg mL^{-1} for *E.coli*) for 4 h. After treatment, the solution was washed with PBS (pH 7.4), followed by staining with SYTO 9 and PI for 15 min and washing to discard excess dye. After that, the samples were imaged using a microscope (Multi-mode reader, CYT5MV, Biotek) with 20× objective magnification with the corresponding excitation and emission filters (469-35/525-39 nm for SYTO^{TM} 9 and 586-15/647-57 nm for propidium iodide).

2.8.4 TEM characterization of bacteria morphology

The bacterial suspensions of *E. coli* or *S. aureus* (≈10^9 CFU mL^{-1}, 1.0 mL) were centrifuged (RCF 3000 g, 10 min, 25 °C) and washed twice with sodium phosphate buffer solution (PBS, pH 7.4). Aliquots (50 μL) of *E. coli* or *S. aureus* suspensions (1.0×10^7 CFU mL^{-1}) were incubated with the CDs and CDs-C9 (CDs at 256 μg mL^{-1} for both strains; CDs-C9 at 16 μg mL^{-1} for *S. aureus* and 32 μg mL^{-1} for *E. coli* in PBS (pH 7.4)) for 4 h and then washed with sodium phosphate solution (pH 7.4; 1.0 mL) to remove the matrix. The samples were carefully deposited on 300-mesh carbon-coated Cu grids followed by fixation with 2.5% glutaraldehyde solution and washing with PBS (pH 7.4). Then, the samples were dried at room temperature for 1 h, and images were observed and collected *via* TEM.
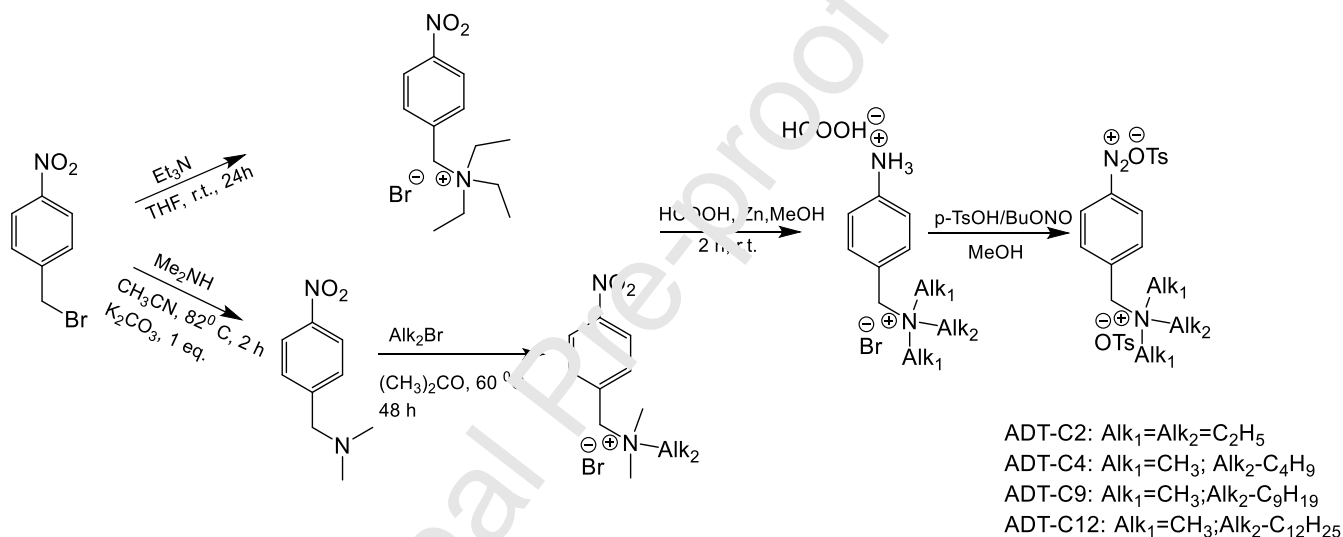
Statistical Analysis. The one-way ANOVA Dunnett's multiple comparisons test with a single pooled variance with a confidence level of 95% is used. The data were analyzed using GraphPad Prism (version 9.3.0) by comparison between treated and untreated groups. P values of 0.05 were considered to be significantly different from the control.

3.   Results and discussion

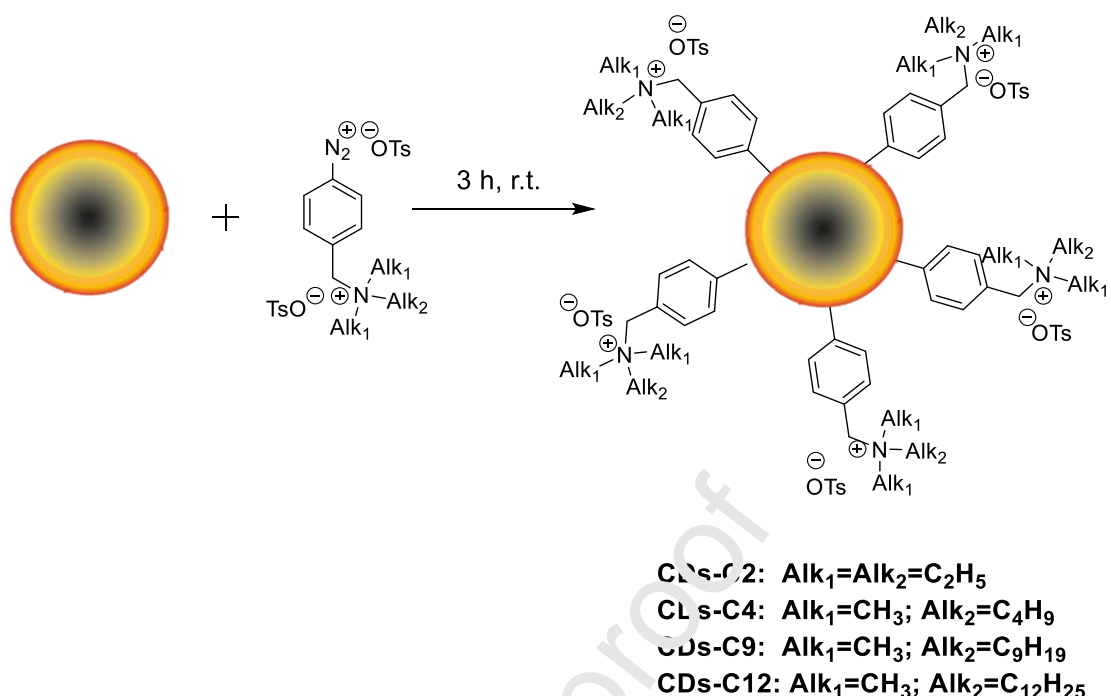### *3.1 Synthesis and characterization of CDs, CDs-C2, CDs-C4, CDs-C9 and CDs-C12*

In the first stage, we synthesized arenediazonium tosylates (ADT-N$^+$Alk$_3$) bearing different alkyl moieties (ethyl (C2), butyl (C4), nonyl (C9) and dodecyl (C12)) with the aim to estimate and clarify the influence of the alkyl chain length on antibacterial properties (**Figure 1**). The different alkyl chains were chosen for the analysis of relationship between the structure of organic functional groups on the CDs surface and antibacterial activity. The short chain groups (ADT-C2 and ADT-C4), owing to their positive charge, are expected to interact with the negatively-charged bacterial cell membrane. The longer chains bring additional hydrophobic interactions. The second reason is

11

related to the commercial availability of the starting materials for the preparation of diazonium salts and related CDs. The synthesis started from the commercially available 4-nitrobenzyl bromide precursor, followed by alkylation with triethylamine (formation of the corresponding triethylammonium salt) or dimethylamine. The *N,N*-dimethyl-*N*-(4-nitrobenzyl)amine was subjected to a second alkylation using appropriate alkyl bromide to yield tetraalkylammonium salts. The simple reduction of NO$_2$ group by Zn-powder in formic acid led to the formation of the desired amine, which was diazotized in the presence of 4-toluenesulfonic acid. The isolated salts **ADT-C2, ADT-C4, ADT-C9** and **ADT-C12** showed enhanced stability at storage and can be used during at least 3 months after the preparation [46].

ADT-C2: Alk$_1$=Alk$_2$=C$_2$H$_5$
ADT-C4: Alk$_1$=CH$_3$; Alk$_2$-C$_4$H$_9$
ADT-C9: Alk$_1$=CH$_3$;Alk$_2$-C$_9$H$_{19}$
ADT-C12: Alk$_1$=CH$_3$;Alk$_2$-C$_{12}$H$_{25}$

Figure 1. Preparation of ADT-C2, C4, C9 and C12 (the experimental procedures are provided in the SI).

CDs were prepared by a fast and facile microwave-assisted approach using citric acid as an environmentally-friendly carbon source and ethylenediamine [26,47] (**Figure S1**). The covalent modification by diazonium salts was carried out *via* simple mixing of CDs and ADT-N$^+$Alk$_3$ solutions under stirring and ultrasonication at room temperature. The resulting products were purified by dialysis **(Figure 2)**.

CDs-C2: Alk$_1$=Alk$_2$=C$_2$H$_5$
CDs-C4: Alk$_1$=CH$_3$; Alk$_2$=C$_4$H$_9$
CDs-C9: Alk$_1$=CH$_3$; Alk$_2$=C$_9$H$_{19}$
CDs-C12: Alk$_1$=CH$_3$; Alk$_2$=C$_{12}$H$_{25}$

Figure 2. Preparation of CD-C2, CDs-C4, CDs-C9 and CDs-C12.

The surface modification by tetraalkylammonium moieties (**TAA**) was proved by Fourier-transform infrared (FTIR) spectroscopy and X-ray photoelectron spectroscopy (XPS). FTIR spectrum of pristine CDs revealed the presence of C=O/N-H deformation (1660 cm^{-1}), C=C (1560 cm^{-1}) and C-N (1400 cm^{-1}) stretching vibrations, consistent with previously reported data [26]. After surface modification, the FTIR spectrum of modified CDs showed the appearance of novel vibration bands associated with covalent attachment of TAA groups: vibrations of alkyl chain (2930-2850, 1360, 685 cm^{-1}), aromatic ring breathing modes (685, 1000, 1124, 1183 cm^{-1}) and tosylate anion (685, 1033, 1124, 1183 cm^{-1}) (**Figure 3A, Figure S2, Table S1**) [48]. The absence of a vibration band at 2300-2230 cm^{-1} (N≡N$^+$) indicates the absence of chemisorbed diazonium cations (**Figure 3A, Figure S2**).
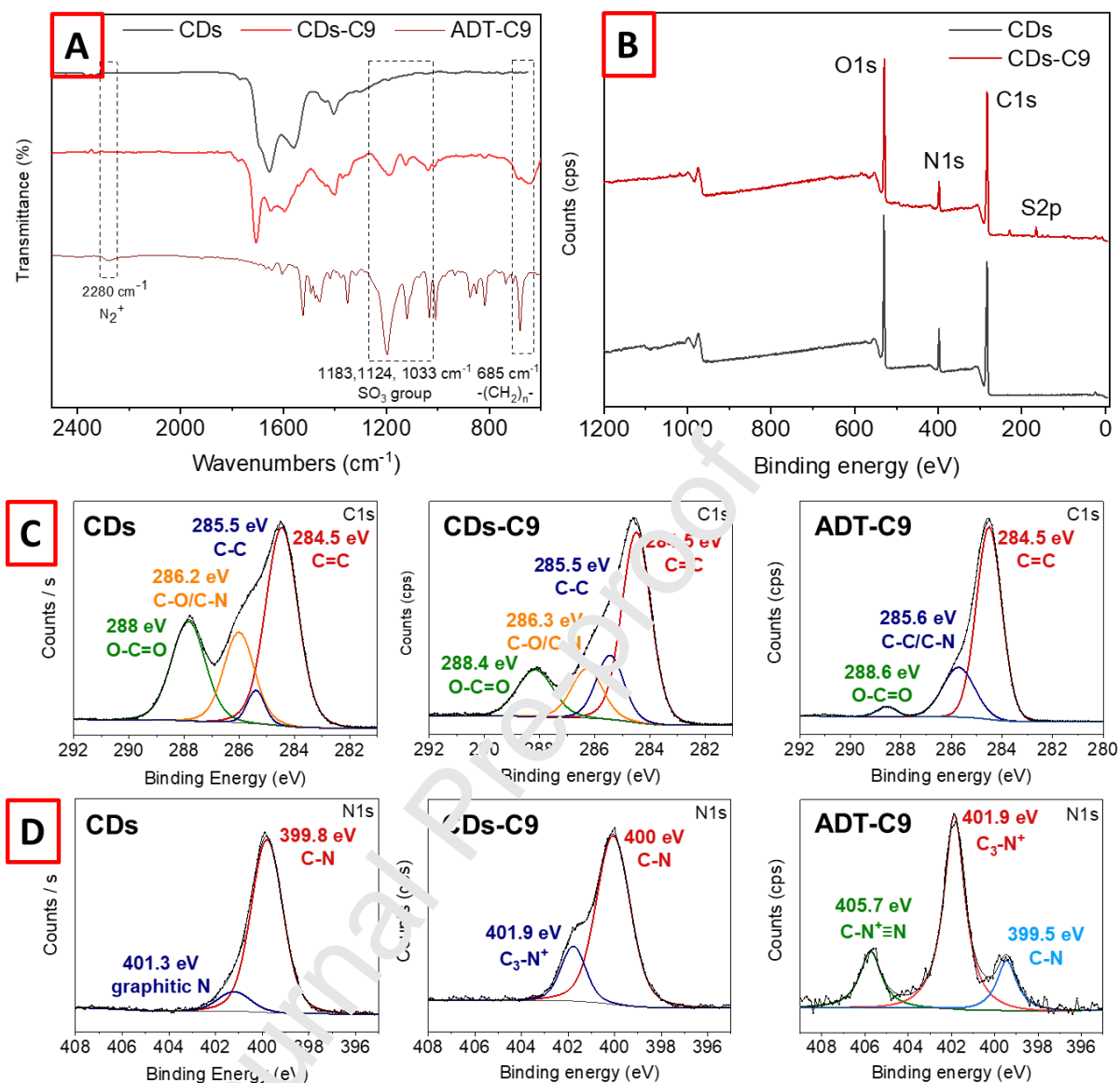
Figure 3. (**A**) FTIR spectra of CDs, CDs-C9 and ADT-C9, (**B**) XPS survey spectra of CDs and CD-C9, and (**C**) core level spectra of the C_{1s} of CDs, CDs-C9 and ADT-C9, and (D) N_{1s} of CDs, CDs-C9 and ADT-C9.

The chemical composition of the pristine and modified CDs was evaluated by XPS analysis (**Figure 3B**). The XPS survey spectrum of pristine CDs displays several peaks at 284.5, 400.0, and 531.0 eV assigned respectively to C_{1s}, N_{1s} and O_{1s}. Compared to pristine CDs, the XPS survey spectra of the modified CDs feature additional peaks due to S_{2p} and S_{2s} at 167.5 and 229.0 eV, respectively, associated with counterion TsO^- of tetraalkylammonium moieties (**Figures 3B, S3, Table S2**) [49]. The deconvolution of the C_{1s} peak allows to identify four components ascribed to C=C/sp² (284.5 eV), C-C (285.5 eV), C-O/C-N (286.5 eV) and O-C=O (288.5 eV) (**Figure 3C**).

14

Moreover, diazonium modification leads to an increase of the C-C component at 285.5 eV from ≈3 to ≈12 at.% and C=C at 284.5 eV for all modified CDs. The deconvolution of the N_{1s} peak (**Figure 3D**) allows to identify the C–N and C_3-N^+ groups at 400.0 and 401.7 eV, respectively. While pristine CDs do not feature C_3-N^+ component, grafting of ADTs-C2-C12 results in its growth up to 1.8 at.%, clearly indicating the presence of TAA groups in the structure of the modified CDs (**Table S2**). The highest increase of C-N, C=C and C_3-N^+ components and S_{2p} concentrations was observed for CDs-C2 and CDs-C9 (**Table S2**). Additional confirmation of covalent grafting of ADTs to CDs is the disappearance of C-N≡N^+ related peak at 405.7 eV due to ADTs [31,38,50].

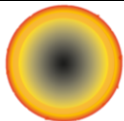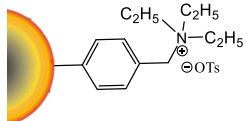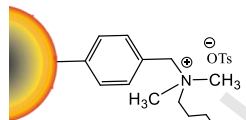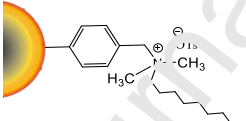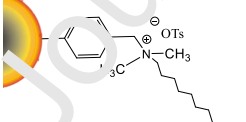Additionally, all prepared materials have been characterized by optical methods, such as UV-vis and fluorescence spectroscopy (**Figure S4**). The UV−vis spectra of pristine CDs exhibited the common absorbance peaks at 253 and 341 nm due to the π–π^* transition of aromatic C=C bond, n→π^* transition of the C=O and C=N bonds, respectively [26] (**Figure S4A**). For the modified CDs, the appearance of a new broad peak at 450 nm, ascribed to agglomeration of weak positively charged CDs (**Table 1**), represents an indirect proof of a new lower energy state from attached functional groups [51] (**Figure S4A**). The fluorescence quantum yield (QY, Φ) of pristine CDs is 0.21 as compared to that of quinine sulfate used as reference (QY, 0.54 in 0.1 M H_2SO_4) (**Figure S4C**). The surface modification suppresses sufficiently the fluorescence, as reported earlier [52] (**Figure S4B,C**). The apparent decrease of the fluorescence peak intensity at 448 nm under 358 nm excitation for the modified CDs compared to pristine is due to the formation of surface layer after modification (**Figure S4B**).

The fluorescence spectra taken at excitations from 320 to 400 nm exhibit an excitation (λ_{ex})-independent emission (λ_{em}) behavior, which may originate from the narrow distribution of several key parameters such as surface defects, band gap, surface structure and diameter size [53,54]. The location of the fluorescence excitation and emission peaks for all modified CDs was slightly blue-shifted and also expressed in higher intensity at an excitation of 340 nm than at 360 nm (**Figure S5**). The shift in fluorescence emission peaks after functionalization originates from the bandgap tuning of the CDs after modification, which is probably due to the formation of new energy levels within the existing band gap structure [55,56].

In addition to chemical and optical characterization, we studied the geometrical and hydrodynamic size of prepared materials by AFM and DLS measurements (**Table 1, Figures S6, S7**). Both methods demonstrated the apparent increase of particles' size upon increasing the alkyl chain length. A significant drop was observed only for CDs-C12 for which the hydrodynamic and

geometrical diameters were similar to those of CDs-C2 and CDs-C4. This fact can be explained by the conformational freedom of long alkyl chain, which can form relatively dense structures in water or on substrates. The attachment of TAA moieties led to a pronounced change of the zeta potential of the pristine CDs from negative value to positive (**Table 1**), facilitating the interaction of modified CDs with negatively charged cell membranes [25,57].

Table 1. ζ-potential and size of CDs and modified CDs.

	Structure	ζ-potential, mV	diameter[a], nm	hydrodynamic diameter[b], nm
CDs		-13.0±3.0	2.5±0.3	7.3±1.7
CDs-C2		+2.7±2.2	4.0±0.8	109.9±39.4
CDs-C4		+4.7±2.5	5.5±0.8	72.1±20.5
CDs-C9		+7.5±2.0	6.5±1.0	130.2±60.8
CDs-C12		+13.0±3.0	3.5±1.2	103.7±18.7

[a] according to AFM measurements on mica substrate (**Figure S6**); [b] size distribution by intensity according to DLS measurements (**Figure S7**).

3.2 Antimicrobial properties and cytotoxicity towards Staphylococcus aureus and Escherichia coli

The antimicrobial activity of the pristine and modified CDs was assessed by the broth minimum inhibitory concentration (MIC) test using Gram-positive *Staphylococcus aureus* ATCC® 43300™ (*S. aureus*) and Gram-negative bacteria *Escherichia coli* K12 MG 1655. (*E. coli*). The evaluation of MIC showed that pristine CDs did not affect the bacterial growth, as expected [26] (**Table 2, S3**).

The covalent attachment of C2-alkyl chain (**CDs-C2**) as well as C4-alkyl chain (**CDs-C4**) did not alter the antibacterial activity for both bacterial strains. This could be related to the weak positive surface charge (+2.7±2.3 and +4.7±2.5 mV, respectively) and relatively low ability of short alkyl chains to interact with bacterial membrane (**Table 1, 2**), in agreement with previously reported results [58,59]. In the opposite, the presence of C9-moieties on the CDs' surface induced increased bacterial death with low MIC values for both strains (3.09±1.10 μg mL^{-1} for *S. aureus* and 7.93±0.17 μg mL^{-1} for *E. coli*) in comparison with previously reported data (**Table S4**). Further increase of the alkyl chain (**CDs-C12**) resulted in increased MIC values, owing to the capability of hydrophobic tails of adhering to one another *via* hydrophobic intermolecular interactions, blocking the electrostatic interactions of positively charged TAA with bacteria and diminishing the antibacterial potency. These findings are in good agreement with previous studies of relationship between alkyl length of tetraalkylammonium salts and antibacterial activity of surface-modified materials [60–66].

Despite high antibacterial activity, biocompatibility of CDs is equally important. Previously, it has been reported that cationic polymers such as polyethylenimine (PEI) and derived carbon dots have a certain degree of toxicity, which stumbled their biomedical applications [64,67]. To investigate the biocompatibility of functionalized CDs-TAA, cytotoxicity study of pristine and modified CDs was performed on the mouse embryonic fibroblast 3T3-L1, HeLa (ATCC® CCL-2™), and hypodiploid human (U-87 MG ATCC® HTB-14™) cell lines using MTT and resazurin assay, respectively (**Figure 4, Figure S8**). In case of mouse embryonic fibroblast 3T3-L1 cell line, there is a tendency for an increase of the toxic effect upon increasing the alkyl chain length from C2 to C12, but low cytotoxicity was observed for CD-C9 in the 4-32 μg mL^{-1} concentration range, which is higher than CDs-C9 MIC value (**Figure 4**). After incubation with CDs modified with alkyldiazonium salts of different chain lengths for 24 h at concentrations up to 25 μg mL^{-1}, the viability of HeLa cells (ATCC® CCL-2™) and hypodiploid human (U-87 MG ATCC® HTB-14^{TM}) was high and approaching 95% for all CDs (**Figure S8**). In general, all CDs-TAA possess good biocompatibility and CDs-C9 with the optimal chain length can combat *S. aureus* and *E. coli* bacteria, thereby showing their great potential for antibiofilm applications.

	Alkyl radical	MIC (μg mL^{-1})	
		S. aureus	*E. coli*
CDs	-	>256	>256

CDs-C2	C_2H_5	>256	>256
CDs-C4	C_4H_9	>256	>256
CDs-C9	C_9H_{19}	**3.09±1.10**	**7.93±0.17**
CDs-C12	$C_{12}H_{25}$	64	256

Table 2. MIC values of the CDs and modified CDs on *S. aureus* and *E. coli*.
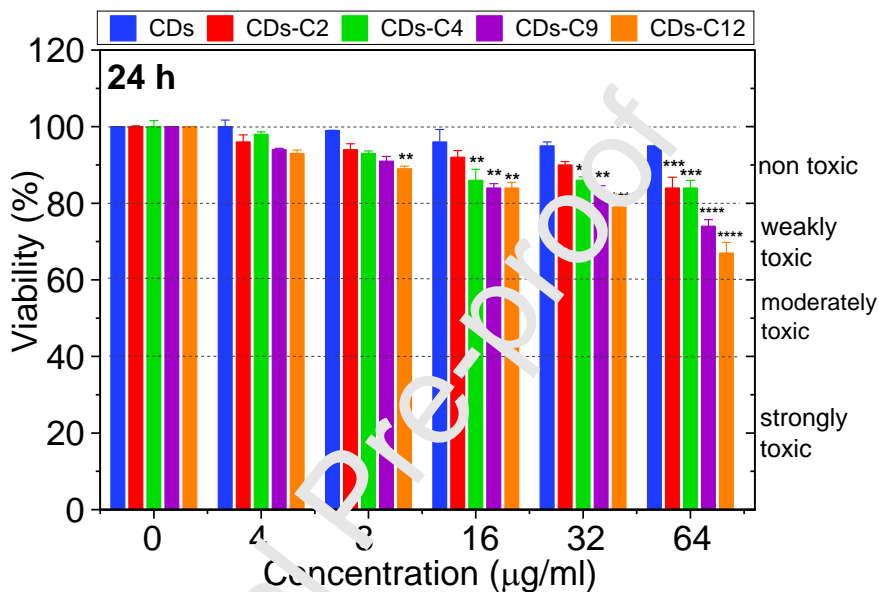

Figure 4. Cell viability of 3T3-L1 cells after 24 h incubation with CDs, CDs-C2, CDs-C4, CDs-C9 and CDs-C12 at different concentrations determined using MTT assay. Error bars represent SD. Significant differences with 100% are indicated (n = 3, **p < 0.01, ***p < 0.001, ****p < 0.0001; as determined by a one-way ANOVA Dunnett's multiple comparisons test with a single pooled variance).

The prepared CDs-C9 outperform most of previously reported CDs in terms of efficacy towards both Gram-positive and negative bacteria with low MIC values (**Table S4**). As was mentioned above, nitrogen-containing compounds are commonly used for the synthesis of antibacterial agents; however, involving alkylamines in hydrothermal synthesis does not provide high antibacterial properties [19,26,68]. In turn, utilization of nitrogen-containing polymers and quaternary ammonium compounds instead of alkylamines enhances the antibacterial properties of the resulting CDs only toward Gram-positive bacteria and still insufficient toward Gram-negative bacteria [23,25,69–71]. The highest antimicrobial properties towards both bacteria was exhibited only by

CDs synthesized from several nitrogen-containing components [24,72]. In comparison with discussed above approaches, covalent grafting of TAA to CDs provides low MIC values for both Gram-positive and negative bacteria combined with simple modification procedure.

3.3 Biofilm destruction activity

The formation of biofilms is one of the most effective mechanisms of resistance of bacterial cells, affecting the antibiotics and host's immune cells penetration and damage [2,73,74]. Previous studies have demonstrated that neutral and anionic CDs cannot penetrate or accumulate efficiently into biofilms [75]. In contrast, amphiphilic particles are able to readily penetrate biofilms [62]. Thus, we evaluated the antibacterial activity of **CDs-C9** towards *S. aureus* and *E. coli* biofilms (**Figure 5**) in the concentration range of 0−256 µg mL^{-1}. The activity was investigated by a series of qualitative (live/dead fluorescence staining) and quantitative (crystal violet (CV) staining assay, spread plate method) methods. Based on published results of biofilm treatment (**Table 3**), we reduced the time of biofilms treatment from 24 h to 6 and 2 h to get closer to practical applications [24,44,76].
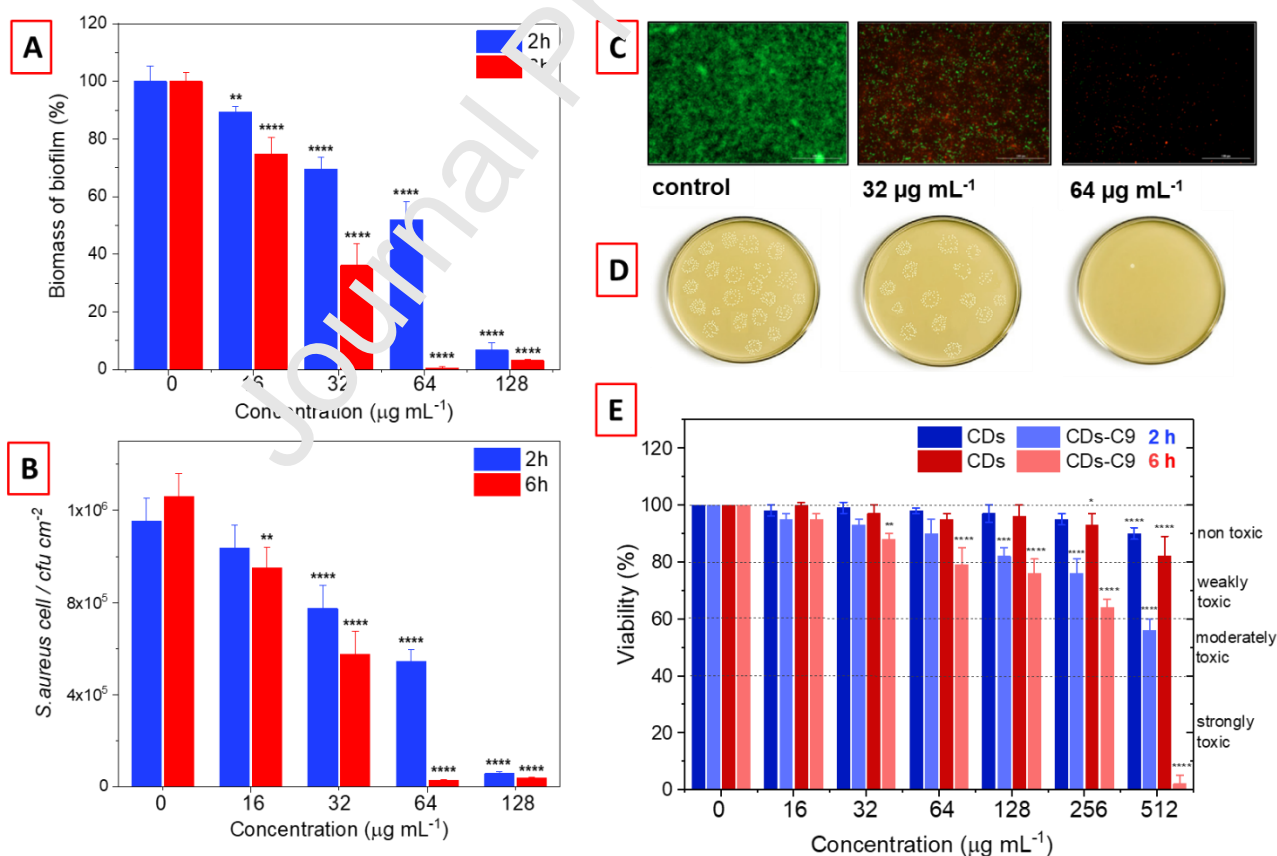
Figure 5. (**A**) Change of the *S. aureus* biomass as a function of CDs-C9 concentration after 2 and 6 h treatment. The biofilm biomass was quantified by the crystal violet (CV) absorbance (OD_{590nm}) of the bacterial biofilms. The biomass of the untreated biofilm was set to be 100%. (**B**) The bacterial survival rate of *S. aureus* in biofilms after 2 and 6 h treatment as a function of CDs-C9 concentration using the spread plate method. (**C**) Live/Dead images of untreated and treated biofilms for 6 h. The bacteria are stained by green and red by SYTO 9/PI. The green and red colors stand for live and dead bacteria, respectively. (**D**) *S. aureus* colonies of bacteria in the biofilm before and after 6 h treatment at treatment at concentrations 0, 32 and 64 μg mL^{-1}. (**E**) Viability of 3T3-L1 cells treated with the pristine CDs and CDs-C9. 3T3-L1 cells were grown in 96-well plates (10^4 cells/well) with 100 μL of culture medium containing increasing concentration of CDs for 2 h (red) and 6 h (blue). The results, expressed as percentage of viability, are the mean value of two independent experiments with each treatment performed in triplicate. Negative control without CDs. Error bars represent SD. Significant differences with 100% are indicated (n = 3, *p < 0.05, **p < 0.01, ****p < 0.0001; as determined by a one-way ANOVA Dunnett's multiple comparisons test with a single pooled variance).

The obtained results revealed that CDs-C9 could obstruct and destroy the biofilms of *S. aureus* in a dose-dependent way. Thus, incubation with CDs-C9 (32 μg mL^{-1}) led to 30% loss of the biofilm mass after 2 h and more than 60% after 6 h of treatment. The mass of the biofilms was less than 5% after treatment with CDs-C9 at 64 μg mL^{-1} for 6 h and at 128 μg mL^{-1} for 2 h that also was proved by the colony formation results (**Figure 5A, B**). The bacterial viability of biofilms decreased with increasing CDs-C9 concentration (bacterial viability rate is <10% at effective concentrations), and the above results are consistent with the results of crystal violet staining (**Figure 5B**). In addition, two-dimensional images of *S. aureus* biofilms stained using the LIVE/DEAD staining assay after 6 h treatment with different concentrations of CDs-C9 demonstrated only dead bacteria (red color) in contrast to live bacteria stained green (**Figure 5C, D**). In short, the obtained results suggest that CD-C9 is a promising agent against *S. aureus* bacterial biofilms. In contrast, previously reported CDs usually require high CDs concentrations and longer treatment times (**Table 3**).

In addition, we evaluated the performance of CDs-C9 towards *E. coli* biofilms (**Figure S9**). After treatment for 6 h with CDs-C9, the biomass of the biofilms was lower than 35% at a concentration of 128 μg mL^{-1} and less than 30% at a concentration of 256 μg mL^{-1}, as determined by the colony formation assay. The weak cytotoxicity at these concentrations (**Figure 5E**) suggests the possibility

20

of CD-C9 utilization not only in natural, industrial, and hospital settings but also for the treatment of biofilm-related infections [77]. Although CDs-C9 demonstrated relatively lower activity towards Gram-negative bacterial biofilms, it was the highest among reported CD-based antibacterial materials [78] (**Table 3**).

Table 3. Comparison of antibiofilm performance of carbon quantum dots.

Antibiofilm agent	Bacteria strains	Biofilm growth conditions	Time of treatment (h)	Working concentration ($\mu g\ mL^{-1}$)	Ref.
CQD$_{2.5w}$	*S. aureus*	24 h	24	250	[69]
N-CQDs	*S. aureus*	48 h	24	20, approximately 70% (upper concentration – toxic)	[24]
CQD$_{180}$	*S. aureus*	24 h	24	80	[76]
CDs-C9	*S. aureus*	72 h	**2**	**128**	Our work
			6	**64**	
	E. coli	120 h	6	**256,** approximately 70% bacteria death	

3.4 Mechanism investigation

The recorded data provide the essential findings for shedding the light on the understanding of the interaction mechanism between bacteria and carbon dots depending on the surface structure and alkyl chain length in TAA.

For understanding the mechanism of bacteria and carbon dots interaction followed by bacteria death, several factors are considered:

(1) generation of reactive oxygen species (ROS), leading to oxidative damage of cells *via* the interaction with cellular components

(2) electrostatic interactions between the negatively-charged bacteria membrane and the positively charged carbon dots;

(3) hydrophobicity of alkyl chain, promoting penetration of CDs into the hydrophobic lipid layers of the cell membrane for further damage;

Previously, it has been reported that carbon materials such as graphene oxide, graphene and carbon quantum dots are able to demonstrate efficient antibacterial properties due to generation of intracellular ROS, followed by oxidative stress and bacteria death [25]. In order to probe the mechanism (1) of ROS formation, the possible generation of intracellular ROS during the interaction of CDs and bacterial cells was evaluated using a 2′,7′-dichlorodihydrofluorescein diacetate (DCFH-DA) assay. The generation of ROS species upon treatment of *E. coli* or *S. aureus* with pristine and modified CDs was not observed at concentrations of 64 μg mL^{-1} (>8-fold MIC for tested bacteria for CDs-C9) (**Figure S10)**. This result means that the antibacterial activity of CDs-C9 associated with the intracellular ROS generation could be excluded.

Thus, the physical membrane disruption through the interaction of hydrophobic alkyl chain became a main hypothesis. In order to prove it, we carried out bright field and fluorescence microscopy after 15 min of incubation *E. coli* and *S. aureus* with CDs to investigate the ability of CDs to attach to the bacteria cell membrane (**Figure S11**). In the case of CDs, CDs-C2 and CDs-C4 we did not observe any changes in bacteria cells distribution, suggesting relatively weak bacteria-CDs interaction. The treatment by CDs-C9 resulted in apparent process of CDs immobilization on the membrane and resulted in strong green fluorescence signal from CDs-C9 for both strains and agglomeration of bacteria. The formation of such agglomerates could also have an impact on the electrical and physical balance of the cell membrane and, in the synergy with a positive charge and the hydrophobic alkyl chain, cause cell death. Moreover, we observed sufficient differences in the interaction of CDs-C9 with Gram-positive (*S. aureus*) and Gram-negative (*E. coli*) bacteria related to the membrane structure. Gram-positive bacteria membrane possesses two-layered structure formed by peptidoglycan and teichoic acids, whereas Gram-negative bacteria possess an outer membrane containing lipopolysaccharides and phospholipids, in addition to the peptidoglycan layer [25]. Indeed, for the Gram-positive *S. aureus,* we observed brighter fluorescence on the membrane surface and sufficient bacteria agglomeration in comparison with *E. coli.* The interaction of CDs-C9 with *S. aureus* are based on electrostatic interactions of positively charged CDs-C9 with the teichoic acid, whereas in *E. coli,* the hydrophobic effects between the lipopolysaccharides layer and alkyl chains are believed to be dominant [79]. In comparison with CDs-C9, interaction with CDs-C12 revealed weaker adsorption on the bacteria cells, resulting in lower number and smaller size of bacteria agglomerates.

The physical damage and morphology of cell membrane after treatment with CDs were also investigated by SYTO^{TM} 9/propidium iodide (PI) staining assay [80] (**Figure 6, S12**) and TEM

analysis (**Figure 7**). The SYTO^{TM} 9 can permeate through the membrane of cells, bind with DNA and then emit green fluorescence, while PI dye can only penetrate the damaged membrane of bacterial cells, stain the nucleus and then emit red fluorescence. Thus, for both strains, the treatment with CDs, CDs-C2 and CDs-C4 did not reveal sufficient damage of the cell membranes, except for CDs-C2 and CDs-C4 for which a few dead cells were observed (**Figure 6, S12**). The treatment with CDs-C12 resulted in appearance of small agglomerates of dead bacteria for both strains, however, live green stained bacteria were observed for the *E. coli* strain. After treatment with CDs-C9, mostly red stained bacteria agglomerates were observed, which proves the key role of the penetration of CDs-C9 into the cell wall, leading to its damage and rupture. TEM analysis of bacteria before and after treatment with CDs-C9 also confirmed the membrane damage. The TEM images (**Figure 7**) of the untreated and treated bacteria with pristine CDs retained a well-defined morphology of clear edge and smooth cell membrane. After treatment with CDs-C9, mostly shapeless agglomerates of wrinkled *S. aureus* bacteria with intracellular leakage were seen (**Figure 7A**). For *E. coli* bacteria, agglomerates of cell membranes and intracellular contents as well as single broken and leaking bacteria were evidenced (**Figure 7B**).
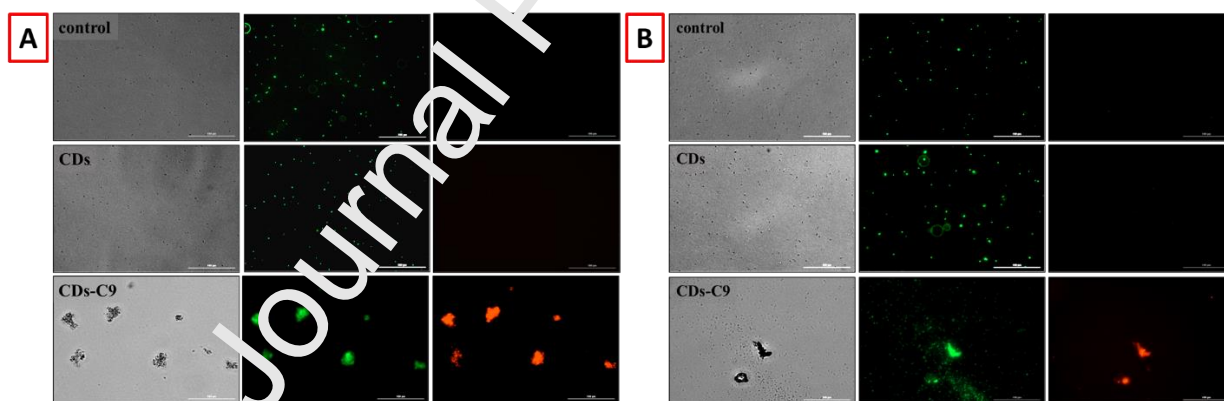
Figure 6. SYTO/PI staining assay of (**A**) *S. aureus* bacteria treated with pristine CDs (256 μg mL^{-1}), CDs-C9 (16 μg mL^{-1}); (**B**) *E. coli* bacteria treated with pristine CDs (256 μg mL^{-1}), CDs-C9 (32 μg mL^{-1}).
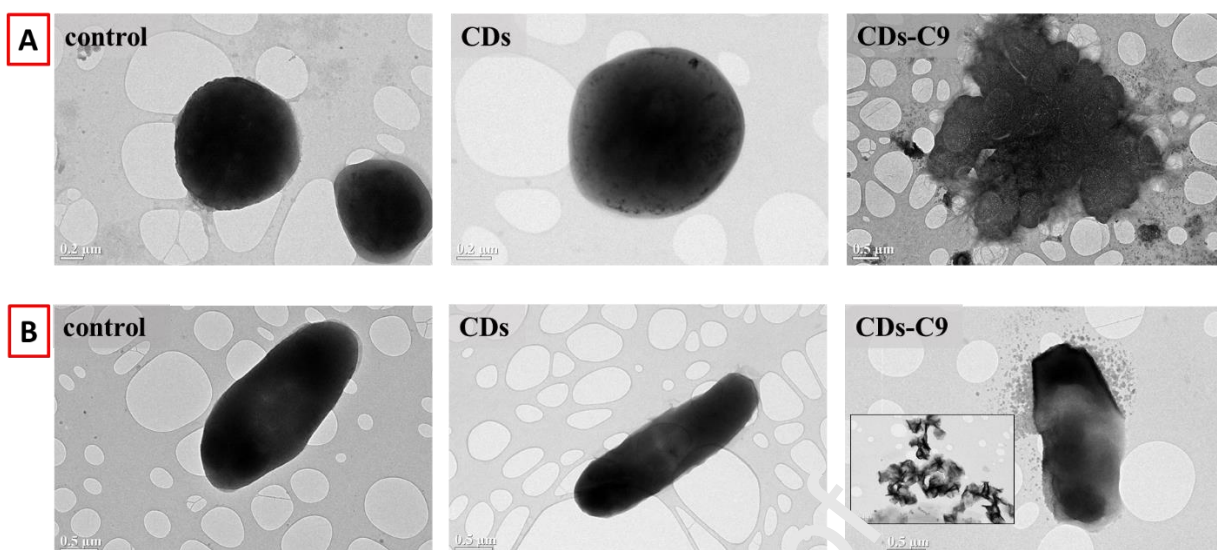
Figure 7. TEM images of (**A**) *S. aureus* before and after treatment with pristine CDs (256 μg mL^{-1}) and CDs-C9 (16 μg mL^{-1}), and (**B**) *E. coli* before and after treatment with pristine CDs (256 μg mL^{-1}) and CDs-C9 (32 μg mL^{-1}).

Therefore, the obtained results suggest that the mechanism of enhanced antibacterial activity of CDs-C9 can be explained by the optimal balance between two main factors: (i) the positive charge on the surface, increasing affinity towards cell membrane and leading to the agglomeration process and membrane balance disturbance and (ii) the hydrophobicity of alkyl chain, promoting penetration of CDs into the hydrophobic lipid layer of the cell membrane for further damage and rupture.

4.   Conclusion

In summary, a versatile functionalization protocol for the covalent attachment of tetraalkylammonium (TAA) moieties onto carbon dots (CDs) surface *via* diazonium surface chemistry was demonstrated. Optimization of the alkyl chain length allowed to achieve a maximum antibacterial efficacy with low MIC values for Gram-positive *S. aureus* (3.09±1.10 μg mL^{-1}) and Gram-negative *E. coli* (7.93±0.17 μg mL^{-1}) bacteria. In addition, CDs-C9 was found to be an efficient agent for the treatment of *S. aureus* biofilms with a full inhibition at a concentration of 64 μg mL^{-1} after 6 h and at 128 μg mL^{-1} after 2 h treatment. Furthermore, the developed material was able to suppress the growth of *E. coli* biofilm: treatment with CDs-C9 (128 μg mL^{-1}) for 6 h led to >60% suppression of biofilm mass. The antibiofilm activity of CDs-C9 outperforms previously

reported CDs in terms of treatment duration and minimal inhibitory concentration. The best antibacterial properties of CDs-C9 was ascribed to the balance between the positive charge and hydrophobicity of the alkyl chains responsible of enhanced interaction with the negatively charged cell membrane, its penetration, disturbance physiological metabolism and its subsequent damage. Besides, the most active CDs-C9 exhibited low cytotoxicity to three cell lines. Our findings provide new effective antimicrobial agent, but also offer an experimental strategy for investigation of structure-antimicrobial activity relationship.

Declaration of competing interest

The authors declare that they have no known competing financial interests or personal relationships that could have appeared to influence the work reported in this paper.

Appendix A. Supporting information

References

[1]   https://www.who.int/news-room/fact-sheets/detail/antimicrobial-resistance.

[2]   D. Sharma, L. Misba, A.U. Khan, Antibiotics versus biofilm: an emerging battleground in microbial communities, Antimicrob. Resist. Infect. Control 8 (2019) 76. https://doi.org/10.1186/s13756-019-0533-3.

[3]   T. Kshetri, D.T. Tran, D.C. Nguyen, N.H. Kim, K. Lau, J.H. Lee, Ternary graphene-carbon nanofibers-carbon nanotubes structure for hybrid supercapacitor, Chem. Eng. J. 380 (2020) 122543. https://doi.org/https://doi.org/10.1016/j.cej.2019.122543.

[4]   Z.L. Shaw, S. Kuriakose, S. Cheeseman, M.D. Dickey, J. Genzer, A.J. Christofferson, R.J. Crawford, C.F. McConville, J. Chapman, V.K. Truong, A. Elbourne, S. Walia,

Antipathogenic properties and applications of low-dimensional materials, Nat. Commun. 12 (2021) 3897. https://doi.org/10.1038/s41467-021-23278-7.

[5]   A. Ivask, T. Titma, M. Visnapuu, H. Vija, A. Kakinen, M. Sihtmae, S. Pokhrel, L. Madler, M. Heinlaan, V. Kisand, R.S. and A. Kahru, Toxicity of 11 Metal Oxide Nanoparticles to Three Mammalian Cell Types *In V_itro*, Curr. Top. Med. Chem. 15 (2015) 1914–1929. https://doi.org/http://dx.doi.org/10.2174/1568026615666150506150109.

[6]   Y. Bi, G. Xia, C. Shi, J. Wan, L. Liu, Y. Chen, Y. Wu, W. Zhang, M. Zhou, H. He, R. Liu, Therapeutic strategies against bacterial biofilms, Fundam. Res. 1 (2021) 193–212. https://doi.org/10.1016/j.fmre.2021.02.003.

[7]   N. Tejwan, A.K. Saini, A. Sharma, T.A. Singh, N. Kumar, J. Das, Metal-doped and hybrid carbon dots: A comprehensive review on their synthesis and biomedical applications, J. Control. Release. 330 (2021) 132–150. https://doi.org/10.1016/j.jconrel.2020.12.023.

[8]   K. Su, L. Tan, X. Liu, Z. Cui, Y. Zheng, B. Li, Y. Han, Z. Li, S. Zhu, Y. Liang, X. Feng, X. Wang, S. Wu, Rapid Photo-Sonotherapy for Clinical Treatment of Bacterial Infected Bone Implants by Creating Oxygen Deficiency Using Sulfur Doping, ACS Nano 14 (2020) 2077–2089. https://doi.org/10.1021/acsnano.9b08686.

[9]   J. Li, Z. Li, X. Liu, C. Li, Y. Zheng, K.W.K. Yeung, Z. Cui, Y. Liang, S. Zhu, W. Hu, Y. Qi, T. Zhang, X. Wang, S. Wu, Interfacial engineering of Bi2S3/Ti3C2Tx MXene based on work function for rapid photo-excited bacteria-killing, Nat. Commun. 12 (2021) 1224. https://doi.org/10.1038/s41467-021-21435-6.

[10]   C. Mao, Y. Xiang, X. Liu, Z. Cui, X. Yang, Z. Li, S. Zhu, Y. Zheng, K.W.K. Yeung, S. Wu, Repeatable Photodynamic Therapy with Triggered Signaling Pathways of Fibroblast Cell Proliferation and Differentiation To Promote Bacteria-Accompanied Wound Healing, ACS Nano 12 (2018) 1747–1759. https://doi.org/10.1021/acsnano.7b08500.

[11]   D.-L. Han, P.-L. Yu, X.-M. Liu, Y.-D. Xu, S.-L. Wu, Polydopamine modified CuS@HKUST for rapid sterilization through enhanced photothermal property and photocatalytic ability, Rare Met. 41 (2022) 663–672. https://doi.org/10.1007/s12598-021-01786-1.

[12]   D. Han, Y. Li, X. Liu, K.W.K. Yeung, Y. Zheng, Z. Cui, Y. Liang, Z. Li, S. Zhu, X. Wang, S. Wu, Photothermy-strengthened photocatalytic activity of polydopamine-modified metal-organic frameworks for rapid therapy of bacteria-infected wounds, J. Mater. Sci. Technol. 62 (2021) 83–95. https://doi.org/10.1016/j.jmst.2020.05.055.

[13]   Y. Luo, X. Liu, L. Tan, Z. Li, K.W.K. Yeung, Y. Zheng, Z. Cui, Y. Liang, S. Zhu, C. Li, X.

Wang, S. Wu, Enhanced photocatalytic and photothermal properties of ecofriendly metal-organic framework heterojunction for rapid sterilization, Chem. Eng. J. 405 (2021) 126730. https://doi.org/10.1016/j.cej.2020.126730.

[14] S. Szunerits, R. Boukherroub, Antibacterial activity of graphene-based materials, J. Mater. Chem. B. 4 (2016) 6892–6912. https://doi.org/10.1039/C6TB01647B.

[15] X. Kong, X. Liu, Y. Zheng, P.K. Chu, Y. Zhang, S. Wu, Graphitic carbon nitride-based materials for photocatalytic antibacterial application, Mater. Sci. Eng. R Reports 145 (2021) 100610. https://doi.org/10.1016/j.mser.2021.100610.

[16] A. Panáček, L. Kvítek, M. Smékalová, R. Večeřová, M. Kolář, M. Röderová, F. Dyčka, M. Šebela, R. Prucek, O. Tomanec, R. Zbořil, Bacterial resistance to silver nanoparticles and how to overcome it, Nat. Nanotechnol. 13 (2018) 65–71. https://doi.org/10.1038/s41565-017-0013-y.

[17] F. Yan, Y. Jiang, X. Sun, Z. Bai, Y. Zhang, X. Zhou, Surface modification and chemical functionalization of carbon dots: a review, Microchim. Acta 185 (2018) 424. https://doi.org/10.1007/s00604-018-2953-9.

[18] H. Feng, Z. Qian, Functional Carbon Quantum Dots: A Versatile Platform for Chemosensing and Biosensing, Chem. Rec. 18 (2018) 491–505. https://doi.org/10.1002/tcr.201700055.

[19] D.I. Abu Rabe, M.M. Al Awak, F. Yang, P.A. Okonjo, X. Dong, L.R. Teisl, P. Wang, Y. Tang, N. Pan, Y.-P. Sun, L. Yang, The dominant role of surface functionalization in carbon dots' photo-activated antibacterial activity., Int. J. Nanomedicine 14 (2019) 2655–2665. https://doi.org/10.2147/IJN.S200493.

[20] H.-J. Jian, R.-S. Wu, T.-Y. Lin, Y.-J. Li, H.-J. Lin, S.G. Harroun, J.-Y. Lai, C.-C. Huang, Super-Cationic Carbon Quantum Dots Synthesized from Spermidine as an Eye Drop Formulation for Topical Treatment of Bacterial Keratitis, ACS Nano 11 (2017) 6703–6716. https://doi.org/10.1021/acsnano.7b01023.

[21] N.A. Travlou, D.A. Giannakoudakis, M. Algarra, A.M. Labella, E. Rodríguez-Castellón, T.J. Bandosz, S- and N-doped carbon quantum dots: Surface chemistry dependent antibacterial activity, Carbon 135 (2018) 104–111. https://doi.org/10.1016/j.carbon.2018.04.018.

[22] Y.-J. Li, S.G. Harroun, Y.-C. Su, C.-F. Huang, B. Unnikrishnan, H.-J. Lin, C.-H. Lin, C.-C. Huang, Synthesis of Self-Assembled Spermidine-Carbon Quantum Dots Effective against Multidrug-Resistant Bacteria, Adv. Healthc. Mater. 5 (2016) 2545–2554. https://doi.org/10.1002/adhm.201600297.

[23] C. Zhao, L. Wu, X. Wang, S. Weng, Z. Ruan, Q. Liu, L. Lin, X. Lin, Quaternary ammonium carbon quantum dots as an antimicrobial agent against gram-positive bacteria for the treatment of MRSA-infected pneumonia in mice, Carbon 163 (2020) 70–84. https://doi.org/10.1016/j.carbon.2020.03.009.

[24] H. Wang, Z. Song, J. Gu, S. Li, Y. Wu, H. Han, Nitrogen-Doped Carbon Quantum Dots for Preventing Biofilm Formation and Eradicating Drug-Resistant Bacteria Infection, ACS Biomater. Sci. Eng. 5 (2019) 4739–4749. https://doi.org/10.1021/acsbiomaterials.9b00583.

[25] X. Hao, L. Huang, C. Zhao, S. Chen, W. Lin, Y. Lin, L. Zhang, A. Sun, C. Miao, X. Lin, M. Chen, S. Weng, Antibacterial activity of positively charged carbon quantum dots without detectable resistance for wound healing with mixed bacteria infection, Mater. Sci. Eng. C 123 (2021) 111971. https://doi.org/10.1016/j.msec.2021.111971.

[26] R. Jijie, A. Barras, J. Bouckaert, N. Dumitrascu, S. Szunerits, R. Boukherroub, Enhanced antibacterial activity of carbon dots functionalized with ampicillin combined with visible light triggered photodynamic effects., Colloids Surf. B. Biointerfaces 170 (2018) 347–354. https://doi.org/10.1016/j.colsurfb.2018.06.040.

[27] K. Rajendiran, Z. Zhao, D.S. Pei, A. Fu, Antimicrobial activity and mechanism of functionalized quantum dots, Polymers 11 (2019). https://doi.org/10.3390/polym11101670.

[28] Q. Dou, X. Fang, S. Jiang, P.L. Chee, T.-C. Lee, X.J. Loh, Multi-functional fluorescent carbon dots with antibacterial and gene delivery properties, RSC Adv. 5 (2015) 46817–46822. https://doi.org/10.1039/C5RA07968C.

[29] C. Cao, Y. Zhang, C. Jiang, M. Qi, G. Liu, Advances on Aryldiazonium Salt Chemistry Based Interfacial Fabrication for Sensing Applications, ACS Appl. Mater. Interfaces 9 (2017) 5031–5049. https://doi.org/10.1021/acsami.6b16108.

[30] O. Guselnikova, P. Postnikov, R. Elashnikov, M. Trusova, Y. Kalachyova, M. Libansky, J. Barek, Z. Kolska, V. Švorčík, O. Lyutakov, Surface modification of Au and Ag plasmonic thin films via diazonium chemistry: Evaluation of structure and properties, Colloids Surfaces A Physicochem. Eng. Asp. 516 (2017) 274–285. https://doi.org/https://doi.org/10.1016/j.colsurfa.2016.12.040.

[31] A.A. Mohamed, Z. Salmi, S.A. Dahoumane, A. Mekki, B. Carbonnier, M.M. Chehimi, Functionalization of nanomaterials with aryldiazonium salts, Adv. Colloid Interface Sci. 225 (2015) 16–36. https://doi.org/10.1016/j.cis.2015.07.011.

[32] A. Bensghaïer, F. Mousli, A. Lamouri, P.S. Postnikov, M.M. Chehimi, The Molecular and

Macromolecular Level of Carbon Nanotube Modification Via Diazonium Chemistry: Emphasis on the 2010s Years, Chem. Africa 3 (2020) 535–569. https://doi.org/10.1007/s42250-020-00144-5.

[33] A.A.L. Ahmad, J.B. Marutheri Parambath, P.S. Postnikov, O. Guselnikova, M.M. Chehimi, M.R.M. Bruce, A.E. Bruce, A.A. Mohamed, Conceptual Developments of Aryldiazonium Salts as Modifiers for Gold Colloids and Surfaces, Langmuir 37 (2021) 8897–8907. https://doi.org/10.1021/acs.langmuir.1c00884.

[34] P. Luo, Z. Ji, C. Li, G. Shi, Aryl-modified graphene quantum dots with enhanced photoluminescence and improved pH tolerance, Nanoscale 5 (2013) 7361. https://doi.org/10.1039/c3nr02156d.

[35] E. Hwang, H.M. Hwang, Y. Shin, Y. Yoon, H. Lee, J. Yang, S. Bak, H. Lee, Chemically modulated graphene quantum dot for tuning the photoluminescence as novel sensory probe, Sci. Rep. 6 (2016) 39448. https://doi.org/10.1038/srep39448.

[36] S. Baghi Sefidan, H. Eskandari, A.N. Shamkhali, Rapid colorimetric flow injection sensing of hypochlorite by functionalized graphene quantum dots, Sensors Actuators B Chem. 275 (2018) 339–349. https://doi.org/10.1016/j.snb.2018.08.023.

[37] C.A. Zuniga, J.B. Goods, J.R. Cox, T.M. Swager, Long-Term High-Temperature Stability of Functionalized Graphene Oxide Nanoplatelets in Arab-D and API Brine, ACS Appl. Mater. Interfaces 8 (2016) 1780–1785. https://doi.org/10.1021/acsami.5b09656.

[38] S. Kesavan, S.A. John, A novel approach to fabricate stable graphene layers on electrode surfaces using simultaneous electroreduction of diazonium cations and graphene oxide, RSC Adv. 6 (2016) 62876–62883. https://doi.org/10.1039/C6RA15821H.

[39] H. Tetsuka, A. Nagoya, T. Fukusumi, T. Matsui, Molecularly Designed, Nitrogen-Functionalized Graphene Quantum Dots for Optoelectronic Devices, Adv. Mater. 28 (2016) 4632–4638. https://doi.org/10.1002/adma.201600058.

[40] S. Zhu, Q. Meng, L. Wang, J. Zhang, Y. Song, H. Jin, K. Zhang, H. Sun, H. Wang, B. Yang, Highly Photoluminescent Carbon Dots for Multicolor Patterning, Sensors, and Bioimaging, Angew. Chemie Int. Ed. 52 (2013) 3953–3957. https://doi.org/10.1002/anie.201300519.

[41] A. Di Martino, P. Kucharczyk, Z. Capakova, P. Humpolicek, V. Sedlarik, Enhancement of temozolomide stability by loading in chitosan-carboxylated polylactide-based nanoparticles, J. Nanoparticle Res. 19 (2017) 71. https://doi.org/10.1007/s11051-017-3756-3.

[42] J.M. Andrews, Determination of minimum inhibitory concentrations, J. Antimicrob.

Chemother. 48 (2001) 5–16. https://doi.org/10.1093/jac/48.suppl_1.5.

[43]   S. Khelissa, A. Gharsallaoui, J. Wang, E. Dumas, A. Barras, C. Jama, F. Jbilou, N. Loukili, N.-E. Chihib, Anti-biofilm activity of dodecyltrimethylammonium chloride microcapsules against Salmonella enterica serovar Enteritidis and Staphylococcus aureus, Biofouling 37 (2021) 49–60. https://doi.org/10.1080/08927014.2021.1873958.

[44]   H.-H. Ran, X. Cheng, Y.-W. Bao, X.-W. Hua, G. Gao, X. Zhang, Y.-W. Jiang, Y.-X. Zhu, F.-G. Wu, Multifunctional quaternized carbon dots with enhanced biofilm penetration and eradication efficiencies, J. Mater. Chem. B 7 (2019) 5104–5114. https://doi.org/10.1039/C9TB00681H.

[45]   M. Budimir, R. Jijie, R. Ye, A. Barras, S. Melinte, A. Silhanek, Z. Markovic, S. Szunerits, R. Boukherroub, Efficient capture and photothermal ablation of planktonic bacteria and biofilms using reduced graphene oxide–polyethyleneimine flexible nanoheaters, J. Mater. Chem. B 7 (2019) 2771–2781. https://doi.org/10.1039/C8TB01676C.

[46]   V.D. Filimonov, M. Trusova, P. Postnikov, E.A. Krasnokutskaya, Y.M. Lee, H.Y. Hwang, H. Kim, K.-W. Chi, Unusually Stable, Versatile, and Pure Arenediazonium Tosylates: Their Preparation, Structures, and Synthetic Applicability, Org. Lett. 10 (2008) 3961–3964. https://doi.org/10.1021/ol8013528.

[47]   C.O. Kappe, Controlled Microwave Heating in Modern Organic Synthesis, Angew. Chemie Int. Ed. 43 (2004) 6250–6284. https://doi.org/10.1002/anie.200400655.

[48]   F. Mirkhalaf, J. Paprotny, D.J. Schiffrin, Synthesis of Metal Nanoparticles Stabilized by Metal−Carbon Bonds, J. Am. Chem. Soc. 128 (2006) 7400–7401. https://doi.org/10.1021/ja058687g.

[49]   H. Wang, P. Sun, S. Cong, J. Wu, L. Gao, Y. Wang, X. Dai, Q. Yi, G. Zou, Nitrogen-doped carbon dots for "green" quantum dot solar cells, Nanoscale Res. Lett. 11 (2016) 1–6. https://doi.org/10.1186/s11671-016-1231-1.

[50]   A. Blacha-Grzechnik, K. Piwowar, P. Koscielniak, M. Kwoka, J. Szuber, J. Zak, Phenothiazines grafted on the electrode surface from diazonium salts as molecular layers for photochemical generation of singlet oxygen, Electrochim. Acta 182 (2015) 1085–1092. https://doi.org/10.1016/j.electacta.2015.10.017.

[51]   Carbonaro, Corpino, Salis, Mocci, Thakkar, Olla, Ricci, On the Emission Properties of Carbon Dots: Reviewing Data and Discussing Models, C — J. Carbon Res. 5 (2019) 60. https://doi.org/10.3390/c5040060.

[52] B. Bin Chen, M.L. Liu, C.M. Li, C.Z. Huang, Fluorescent carbon dots functionalization, Adv. Colloid Interface Sci. 270 (2019) 165–190. https://doi.org/10.1016/j.cis.2019.06.008.

[53] S. Zhu, Y. Song, X. Zhao, J. Shao, J. Zhang, B. Yang, The photoluminescence mechanism in carbon dots (graphene quantum dots, carbon nanodots, and polymer dots): current state and future perspective, Nano Res. 8 (2015) 355–381. https://doi.org/10.1007/s12274-014-0644-3.

[54] H. Ding, X.-H. Li, X.-B. Chen, J.-S. Wei, X.-B. Li, H.-M. Xiong, Surface states of carbon dots and their influences on luminescence, J. Appl. Phys. 127 (2020) 231101. https://doi.org/10.1063/1.5143819.

[55] U. Baruah, M.J. Deka, D. Chowdhury, Reversible on/off switching of fluorescence via esterification of carbon dots, RSC Adv. 4 (2014) 36917 https://doi.org/10.1039/C4RA04734F.

[56] G. Sandeep Kumar, R. Roy, D. Sen, U.K. Ghorai, R. Thapa, N. Mazumder, S. Saha, K.K. Chattopadhyay, Amino-functionalized graphene quantum dots: origin of tunable heterogeneous photoluminescence, Nanoscale 6 (2014) 3384. https://doi.org/10.1039/c3nr05376h.

[57] T.J. Silhavy, D. Kahne, S. Walker, The Bacterial Cell Envelope, Cold Spring Harb. Perspect. Biol. 2 (2010) a000414–a000414. https://doi.org/10.1101/cshperspect.a000414.

[58] F. Li, M.D. Weir, H.H.K. Xu, Effects of Quaternary Ammonium Chain Length on Antibacterial Bonding Agents, J. Dent. Res. 92 (2013) 932–938. https://doi.org/10.1177/0022034513502053.

[59] K. Zhang, L. Cheng, M.D. Weir, Y.-X. Bai, H.H. Xu, Effects of quaternary ammonium chain length on the antibacterial and remineralizing effects of a calcium phosphate nanocomposite, Int. J. Oral Sci. 8 (2016) 45–53. https://doi.org/10.1038/ijos.2015.33.

[60] X. Lv, C. Liu, S. Song, Y. Qiao, Y. Hu, P. Li, Z. Li, S. Sun, Construction of a quaternary ammonium salt platform with different alkyl groups for antibacterial and biosensor applications, RSC Adv. 8 (2018) 2941–2949. https://doi.org/10.1039/C7RA11001D.

[61] S. V. Sapozhnikov, A.E. Sabirova, N. V. Shtyrlin, A.Y. Druk, M.N. Agafonova, M.N. Chirkova, R.R. Kazakova, D.Y. Grishaev, T. V. Nikishova, E.S. Krylova, E. V. Nikitina, A.R. Kayumov, Y.G. Shtyrlin, Design, synthesis, antibacterial activity and toxicity of novel quaternary ammonium compounds based on pyridoxine and fatty acids, Eur. J. Med. Chem. 211 (2021) 113100. https://doi.org/10.1016/j.ejmech.2020.113100.

[62] A. Chen, A. Karanastasis, K.R. Casey, M. Necelis, B.R. Carone, G.A. Caputo, E.F. Palermo,

Cationic Molecular Umbrellas as Antibacterial Agents with Remarkable Cell-Type Selectivity, ACS Appl. Mater. Interfaces 12 (2020) 21270–21282. https://doi.org/10.1021/acsami.9b19076.

[63] M. Benkova, O. Soukup, L. Prchal, R. Sleha, T. Eleršek, M. Novak, K. Sepčić, N. Gunde-Cimerman, R. Dolezal, V. Bostik, P. Bostik, J. Marek, Synthesis, Antimicrobial Effect and Lipophilicity- Activity Dependence of Three Series of Dichained N - Alkylammonium Salts, ChemistrySelect 4 (2019) 12076–12084. https://doi.org/10.1002/slct.201902357.

[64] P.Y.M. Yew, P.L. Chee, O. Cally, K. Zhang, S.S. Liow, X.J. Loh, Quarternized Short Polyethylenimine Shows Good Activity against Drug-Resistant Bacteria, Macromol. Mater. Eng. 302 (2017) 1700186. https://doi.org/10.1002/mame.201700186.

[65] H.-W. Chien, Y.-Y. Chen, Y.-L. Chen, C.-H. Cheng, J.-C. Lin, Studies of PET nonwovens modified by novel antimicrobials configured with both N -halamine and dual quaternary ammonium with different alkyl chain length, RSC Adv. 9 (2019) 7257–7265. https://doi.org/10.1039/C9RA00094A.

[66] M. Chrószcz, I. Barszczewska-Rybarek, Nanoparticles of Quaternary Ammonium Polyethylenimine Derivatives for Application in Dental Materials, Polymers 12 (2020) 2551. https://doi.org/10.3390/polym12112551.

[67] M. Havrdova, K. Hola, J. Skopalik, K. Tomankova, M. Petr, K. Cepe, K. Polakova, J. Tucek, A.B. Bourlinos, R. Zboril, Toxicity of carbon dots – Effect of surface functionalization on the cell viability, reactive oxygen species generation and cell cycle, Carbon 99 (2016) 238–248. https://doi.org/10.1016/j.carbon.2015.12.027.

[68] F. Du, S. Shuang, Z. Guo, X. Gong, C. Dong, M. Xian, Z. Yang, Rapid synthesis of multifunctional carbon nanodots as effective antioxidants, antibacterial agents, and quercetin nanoprobes, Talanta 206 (2020) 120243. https://doi.org/10.1016/j.talanta.2019.120243.

[69] P. Li, X. Yang, X. Zhang, J. Pan, W. Tang, W. Cao, J. Zhou, X. Gong, X. Xing, Surface chemistry-dependent antibacterial and antibiofilm activities of polyamine-functionalized carbon quantum dots, J. Mater. Sci. 55 (2020) 16744–16757. https://doi.org/10.1007/s10853-020-05262-6.

[70] S. Demirci, A.B. McNally, R.S. Ayyala, L.B. Lawson, N. Sahiner, Synthesis and characterization of nitrogen-doped carbon dots as fluorescent nanoprobes with antimicrobial properties and skin permeability, J. Drug Deliv. Sci. Technol. 59 (2020) 101889. https://doi.org/10.1016/j.jddst.2020.101889.

[71] J. Yang, G. Gao, X. Zhang, Y.-H. Ma, X. Chen, F.-G. Wu, One-step synthesis of carbon dots with bacterial contact-enhanced fluorescence emission: Fast Gram-type identification and selective Gram-positive bacterial inactivation, Carbon 146 (2019) 827–839. https://doi.org/10.1016/j.carbon.2019.02.040.

[72] M. Gagic, S. Kociova, K. Smerkova, H. Michalkova, M. Setka, P. Svec, J. Pribyl, J. Masilko, R. Balkova, Z. Heger, L. Richtera, V. Adam, V. Milosavljevic, One-pot synthesis of natural amine-modified biocompatible carbon quantum dots with antibacterial activity, J. Colloid Interface Sci. 580 (2020) 30–48. https://doi.org/10.1016/j.jcis.2020.06.125.

[73] D. Lebeaux, J.-M. Ghigo, C. Beloin, Biofilm-Related Infections: Bridging the Gap between Clinical Management and Fundamental Aspects of Recalcitrance toward Antibiotics, Microbiol. Mol. Biol. Rev. 78 (2014) 510–543. https://doi.org/10.1128/MMBR.00013-14.

[74] J.M. V. Makabenta, A. Nabawy, C.-H. Li, S. Schmidt-Malan, R. Patel, V.M. Rotello, Nanomaterial-based therapeutics for antibiotic-resistant bacterial infections, Nat. Rev. Microbiol. 19 (2021) 23–36. https://doi.org/10.1028/s41579-020-0420-1.

[75] X. Li, Y.-C. Yeh, K. Giri, R. Mout, R.F. Landis, Y.S. Prakash, V.M. Rotello, Control of nanoparticle penetration into biofilms through surface design, Chem. Commun. 51 (2015) 282–285. https://doi.org/10.1039/C4CC07737G.

[76] P. Li, S. Liu, W. Cao, G. Zhang, X. Yang, X. Gong, X. Xing, Low-toxicity carbon quantum dots derived from gentamicin sulfate to combat antibiotic resistance and eradicate mature biofilms, Chem. Commun. 56 (2020) 2316–2319. https://doi.org/10.1039/C9CC09223D.

[77] L. Hall-Stoodley, J.W. Costerton, P. Stoodley, Bacterial biofilms: from the Natural environment to infectious diseases, Nat. Rev. Microbiol. 2 (2004) 95–108. https://doi.org/10.1038/nrmicro821.

[78] F. Lin, C. Li, L. Dong, D. Fu, Z. Chen, Imaging biofilm-encased microorganisms using carbon dots derived from L. plantarum, Nanoscale 9 (2017) 9056–9064. https://doi.org/10.1039/C7NR01975K.

[79] H.H. Tuson, D.B. Weibel, Bacteria–surface interactions, Soft Matter. 9 (2013) 4368. https://doi.org/10.1039/c3sm27705d.

[80] L. Boulos, M. Prévost, B. Barbeau, J. Coallier, R. Desjardins, LIVE/DEAD® BacLight™: application of a new rapid staining method for direct enumeration of viable and total bacteria in drinking water, J. Microbiol. Methods 37 (1999) 77–86. https://doi.org/10.1016/S0167-7012(99)00048-2.

Author Statement

Elizaveta Sviridova - Methodology, Investigation, Visualization, Writing - Original Draft; *Alexandre Barras* - Methodology, Investigation, Validation, Writing - Review & Editing; *Ahmed Addad* - Investigation, Data Curation; *Evgenii Plotnikov* – Methodology, Data Curation; *Antonio Di Martino* - Investigation, Data Curation, Resources; *Dominique Deresmes* - Investigation, Validation, Resources; *Ksenia Nikiforova* - Methodology, Investigation, Resources; *Marina Trusova* – Conceptualization, Supervision, Resources; *Sabine Szunerits* - Validation, Methodology, Writing – Review & Editing; *Olga Guselnikova* Methodology, Investigation, Data Curation, Writing - Review & Editing; *Pavel Postnikov* - Conceptualization, Supervision, Resources, Writing - Review & Editing; *Rabah Boukherroub* - Conceptualization, Supervision, Resources, Writing - Review & Editing

Declaration of interests

☒ The authors declare that they have no known competing financial interests or personal relationships that could have appeared to influence the work reported in this paper.

☐The authors declare the following financial interests/personal relationships which may be considered as potential competing interests:

Highlights

- Facile functionalization of carbon dots by tetraalkylammonium moieties using diazonium chemistry
- Optimization of antibacterial activity by varying different alkyl chains of tetraalkylammonium moieties
- Low MIC values for Gram-positive *S. aureus* (3.09 ± 1.10 µg mL^{-1}) and Gram-negative *E. coli* (7.93 ± 0.17 µg mL^{-1})
- Full biofilm inhibition was achieved after 6 h (64 µg mL^{-1}) and 2 h (128 µg mL^{-1}) treatment for *S. aureus* biofilm
- More than 60% suppression of biofilm mass was achieved after 6 h (128 µg mL^{-1}) treatment for *E. coli* biofilm